Temporal and spatially resolved laser-scattering plasma diagnostics for the characterization of a ms-pulsed glow discharge

Gerardo Gamez,[a] Annemie Bogaerts[b] and Gary M. Hieftje*[a]

Received 18th August 2005, Accepted 16th January 2006
First published as an Advance Article on the web 26th January 2006
DOI: 10.1039/b511764j

A previously described instrument was used to obtain axial profiles of the gas-kinetic temperature (T_g) in a ms-pulsed glow discharge *via* Rayleigh scattering. In addition, the electron number density (n_e) and the electron temperature (T_e) were observed *via* Thomson scattering. For these measurements, the detection optics of the original instrument were modified and a photon-counting imaging technique was employed to allow the simultaneous observation of Thomson scattering from multiple spatial positions. It was found that the cell pressure and electrical characteristics of the glow-discharge pulse have an effect on the temporal behavior of all fundamental parameters. As with a dc glow discharge, there were two distinct classes of electrons, a high-energy group and a lower-energy (thermalized) group. The thermalized electrons showed greater energies during the prepeak than at the plateau. Following the power pulse, during the afterglow, n_e and T_e declined monotonically at the temporal and spatial positions observed. The spatial differences in n_e during the afterglow are discussed with regards to the spatial variations in argon metastable population.

Introduction

Glow discharges have become popular because of their ability to perform direct elemental analysis of solid samples and their superb depth resolution.[1–3] Of late, glow discharges operated in pulsed mode have drawn special attention because they offer several analytical advantages. For instance, pulsing the glow discharge power lowers the degree of cathode heating, which has been shown to affect the global electrical and analytical characteristics of the discharge.[4–6] This allows the use of higher instantaneous powers, which in turn leads to enhanced sputter atom yield, excitation and ionization.[7] In addition, it has been shown that during the discharge pulse the plasma goes through different temporal regimes in which the ionization and excitation conditions change, thus offering very fast tunability.[8,9] Several advantages result from careful selection of the sampling time of the analyte species of interest: lower levels of background species, including isobaric interferences with the analyte,[10] as in the case of the mass spectrometric detection of $^{40}Ca^+$ in the presence of $^{40}Ar^+$; in addition, one can obtain different kinds of qualitative and quantitative information from an analyte, such as elemental, structural, and molecular data, which represents very fast speciation analysis. Because this information is available on a very fast time frame (μs to ms), there is great potential for transient analysis such as in chromatographic detection.[11–15]

Despite these clear analytical advantages, pulsed glow discharges have not been as widely studied as their dc or rf counterparts; we are therefore still far from completely understanding the fundamental plasma processes. In addition, most of the fundamental studies on analytical pulsed glow discharges have focused on the observation or modeling of the temporal and spatial evolution of plasma-gas and cathode-sputtered species *via* absorption, emission or mass spectrometry.[16–24] There have also been some studies in which a thermometric moiety has been introduced into the pulsed discharge in order to follow the internal energy changes as a function of time and position.[25]

In order to improve the glow discharge analytical performance, however, it is important also to obtain a good picture of the temporal and spatial behavior of the fundamental parameters of the pulsed glow discharge; these parameters include the gas-kinetic temperature (T_g), electron number density (n_e), electron energy distribution function (EEDF), and electron temperature (T_e). Observing the electron behavior, for example, will provide information on ionization, excitation and sputtering processes. In addition, characterizing the gas-kinetic temperature will yield information on the global electrical characteristics since this parameter is related to the gas density and this in turn will affect collisions among plasma species. The processing-plasma industry is well aware of the importance of knowing the plasma fundamental parameters and a number of studies can be found for pulsed discharges used in surface-treatment processes, *i.e.*, nitriding plasmas.[26–28] In spite of this fact, fundamental-parameter studies of analytical pulsed glow discharges are very scarce[19,29] and, although the studies from processing plasmas are informative, trying to apply their observations directly would be inaccurate because the experimental conditions and cell arrangements are vastly different.

There are several techniques that can be used to obtain the plasma fundamental parameters. These techniques include Langmuir probes, Stark broadening of the H_β line, Doppler broadening of plasma-gas spectral lines, Boltzmann plots, use

[a] *Department of Chemistry, Indiana University, Bloomington, IN 47405, USA. E-mail: hieftje@indiana.edu.*
[b] *Department of Chemistry, University of Antwerp, Universiteitsplein 1, B-2610 Wilrijk, Antwerp, Belgium*

of thermometric species, and others.[30,31] Unfortunately, these methods suffer several disadvantages, such as perturbing the plasma, requiring the assumption of local thermodynamic equilibrium or the need to perform Abel inversion (a technique that introduces error) to obtain radially resolved values.

An alternative is to use laser scattering techniques such as Rayleigh scattering to study the T_g and Thomson scattering to observe the electron behavior.[32–36] These methods are non-invasive. Other advantages include inherent temporal (limited by the laser pulse width) and spatial resolution. Both techniques are easily coupled to each other: the electron number density and electron temperature are obtained independently (the error is not carried over), and the electron energy distribution function can be acquired directly from the shape of the Thomson-scattering spectra. On the other hand, the laser power needs to be held below a certain threshold to prevent plasma heating, the Thomson scattering signals are very weak due to the small scattering cross sections of the electrons, and it is not an easy technique to implement. Thomson scattering, however, has been recognized as one of the most reliable plasma diagnostics techniques.[35,36]

Recently, an instrument for laser-scattering diagnostics of analytical glow discharges was designed in our laboratory.[37] It has been used successfully to observe the effect of operating conditions on the fundamental parameters of a planar-cathode dc glow discharge.[38,39] The purpose of the present study is to use this same instrument in a time-resolved mode to characterize the transient behavior of the fundamental parameters of a millisecond-pulsed glow discharge under operating conditions appropriate for analytical spectrochemistry. Measurements are focused on the negative glow region and on observation times characteristic of the prepeak, plateau and afterglow temporal regions of the discharge.

Experimental

The laser-scattering instrument used for this study has been described earlier in some detail.[37–39] In short, a frequency-doubled Nd:YAG laser (532 nm) beam is directed into the glow-discharge cell, which features Brewster windows, baffles and a viewing dump to hold stray light to a minimum. The glow discharge has a planar copper cathode (12 mm diameter) and a planar stainless-steel anode (50 mm diameter), held 50 mm apart. The discharge is oriented vertically with the cathode above the anode. The cathode is water-cooled with a chiller set at 13 °C. The laser pulse ($\sim$10 ns) probes the plasma perpendicular to its axis and the scattering is collected at a 135° angle (in the backward direction, *cf*. Fig. 1). The laser power is monitored throughout the experiment for normalization purposes. The plasma gas is Ar (99.997%). The instrument features a double monochromator to minimize stray light and a gated photon-counting system.

The pulsed glow discharge was powered by a high-voltage power supply (BHK 1000-0.2MG, KEPCO Inc.) connected to a high-voltage pulse generator (PVX-4140, Directed Energy Inc.). A digital delay/pulse generator (PDG-2510, Directed Energy Inc.) was used to drive the high-voltage pulse generator and the laser synchronously. The mode of operation

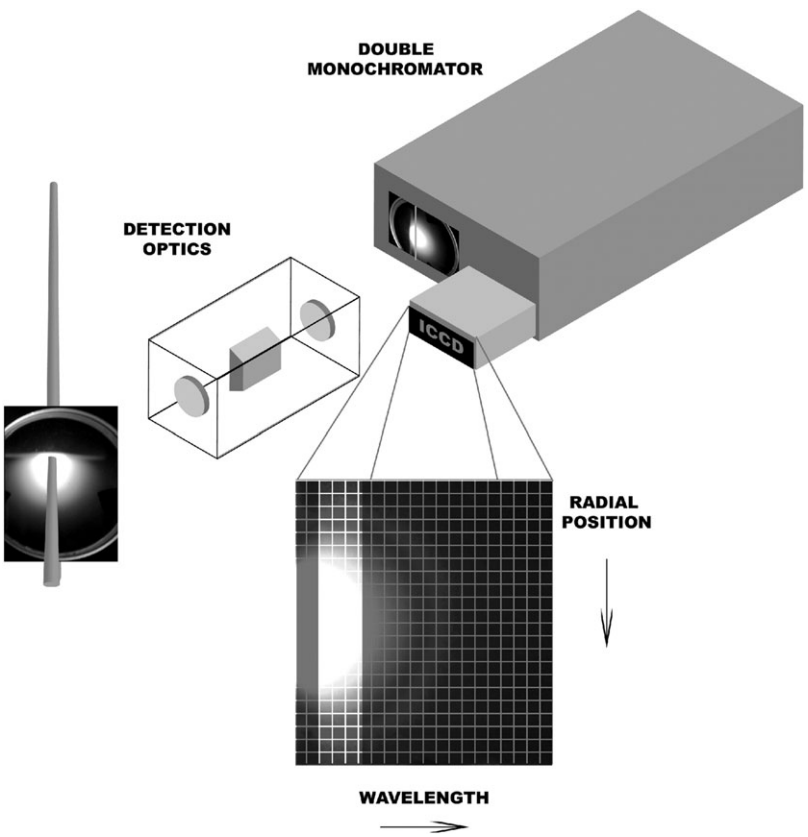

Fig. 1 Schematic diagram of the laser scattering multi-channel gated photon-counting imaging system.

was dc pulsed and the pulse width was 5 ms. The repetition frequency of the glow-discharge pulses was chosen to maximize the laser pulse (20 Hz) to discharge pulse overlap (60 Hz) while keeping frequencies comparable to those used in previous fundamental studies. Thus, a more time-efficient data collection can be achieved. The electrical characteristics and timing were followed throughout the experiment with a digital oscilloscope (TDS 2024, Tektronix Inc.), a high-voltage probe placed before the glow-discharge cathode assembly (80K-6, Fluke Corporation), and a 1.8 Ω resistor placed in series after the anode assembly for current measurement.

For the Thomson-scattering experiments, a multi-channel photon-counting imaging system was assembled in order to collect laser scattering simultaneously from multiple positions within the glow discharge. There are several examples in the literature in which multi-channel Thomson scattering has been successfully performed.[35,40–43] For example, spectrographs and triple polychromators coupled to intensified charge-coupled devices (ICCD) have been used for this purpose.[40,41,43] However, the present study has several requirements that narrow the possibilities. Minimization of stray light becomes especially important in glow-discharge Thomson scattering because of the low electron number densities (compared with other plasmas, *e.g.*, ICP), which will result in weak scattering signals. As was mentioned earlier, the glow-discharge laser-scattering instrument in our laboratory utilizes a double monochromator to minimize stray light. Unfortunately, if this were to be used as a spectrograph, one would have to open the intermediate slits, which would result in an unacceptable loss of stray-light rejection. In the multi-channel configuration in the present study, the ICCD (PI MAX, 512 × 512, Princeton Instruments Inc.) has been fitted with a mask with a viewing window that serves as a slit. In this fashion, the double monochromator serves to pass only a specific wavelength channel (0.3 nm wide, defined by the window of the ICCD mask). The mask allows one to obtain Thomson-scattering photon-event data close to the laser wavelength without the detector being swamped by Rayleigh scattering.

The collection optics are similar to those described by Sesi and co-workers for Thomson scattering from an ICP.[43] They are composed of a front iris to restrict collection of stray light, a lens (50.8 mm diameter, 200.0 mm focal length, BK7) to collimate the image onto a dove prism (30 × 30 × 127 mm, BK7) that rotates the collimated image through an angle of 90°, another iris to match the *f*-number of the double monochromator, followed by a lens (50.8 mm diameter, 100.0 mm focal length, BK7) that focuses the image onto the entrance slit. Because the discharge and laser-beam images are rotated by 90° laser scattering coming from a horizontal slice of the plasma appears parallel to the height of the entrance slit (*cf.* Fig. 1). In this fashion, the spatial information is obtained from the vertical axis of the ICCD. Nevertheless, the wavelength still must be scanned in order to obtain full Thomson-scattering spectra.

The ICCD was operated in a gated photon-counting mode.[41,42,44] For this purpose, a variable delay trigger from the laser Q-switch was used to drive the gating system of the ICCD (gate delay 85 ns, gate width 35 ns) and an appropriate gain was chosen for the microchannel plate (MCP) intensifier to produce the best signal-to-background ratio. A total of 100 laser shots per exposure were accumulated on the CCD in order to maintain a practical experiment and data-analysis time without saturation effects. An image analysis routine was developed in VPascal (V++, Digital Optics Limited, New Zealand) to determine the occurrence of photon events based on a user-selected intensity threshold value. A centroiding algorithm was included in the image analysis routine to determine the photon event pixel position because a single photon hitting the MCP will cause the 'splashing' of multiple electrons at the detector end which will result in the spreading of the signal among adjacent pixels on the CCD. All laser scattering experiments were performed in triplicate.

Results and discussion

Electrical characteristics

The electrical characteristics of the glow-discharge pulse have a strong influence on the temporal behavior of the plasma species.[18] Fig. 2 shows representative shapes of the voltage and current traces at 1 Torr and 3 Torr while the power supply was voltage-controlled or current-limited. When the power supply is voltage-controlled it means that the voltage is set to a determined value and the current is allowed to adjust accordingly, while the opposite holds true for the current-limited case. All voltage traces in Fig. 2 are on the same scale. It can be seen that the voltage traces in the voltage-limited case (Fig. 2A and 2B) follow more closely the shape of the input square-wave pulse. In contrast, when the current is limited (Fig. 2C and 2D) the voltage starts at a high value and falls gradually until the pulse terminates. Similar behavior is observed for the current traces, which are, however, not on the same scale to facilitate a comparison of their shapes. Again, square-wave behavior is more closely followed in the voltage-controlled case (Fig. 2E and 2F) than in the current-limited situation (Fig. 2G and 2H). The ringing at the beginning of the current traces at 3 Torr (Fig. 2E and 2G) can also be observed on the pulser-voltage monitor (data not shown), which indicates it originates in the source. A reproducible spike was observed at the beginning of all the current traces, but it returns to the plateau value at around 0.2 ms. These spikes have also been observed in the current waveforms during plasma immersion ion implantation[45,46] and were suggested to be due to a displacement current. The displacement, or capacitive, current results when a rapid increase/decrease in applied voltage induces an equivalent capacitive load from the components, such as a vacuum chamber, ion matrix sheath (sheath left behind when the electrons adjacent to the cathode surface are repelled), and the electrical circuit.[45,46] Thus, there is a possibility that a displacement-current component might also be contributing to the total current under our experimental conditions. The laser-scattering diagnostic measurements were performed while the pulsed glow discharge was operated in a voltage-controlled mode because no real plateau was observed in the current-limited case. At both 1 and 3 Torr the plateau voltage was 920 V. The plateau current at 3 Torr was 75 mA and at 1 Torr was 13 mA. It is noteworthy that at the beginning of the pulse at 3 Torr the current takes a little longer to stabilize and return to the plateau current. The

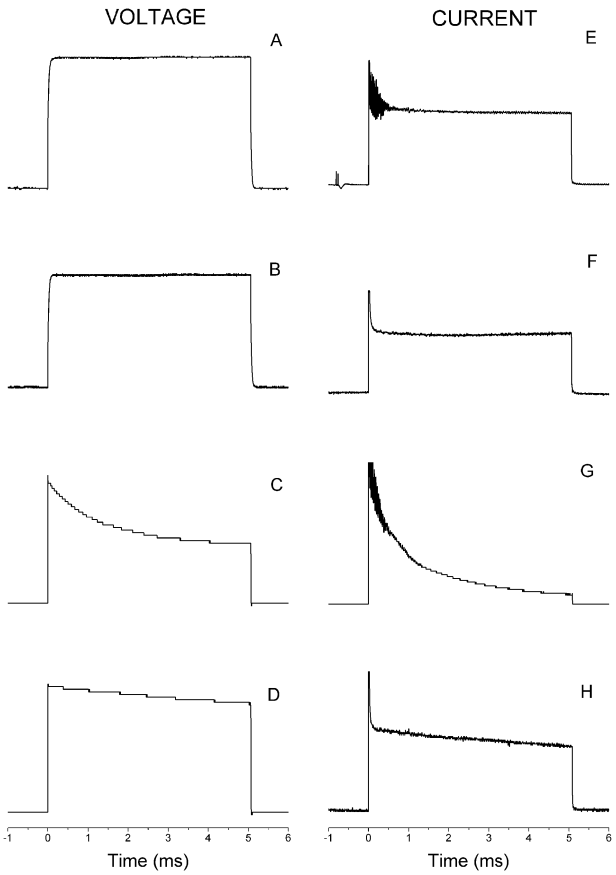

Fig. 2 Voltage and current oscilloscope traces of the glow-discharge pulse under different conditions. Voltage-controlled at 3 Torr (A, E) and 1 Torr (B, F); current-limited at 3 Torr (C, G) and 1 Torr (D, H).

current and voltage RSDs within one experiment were below 5%. The RSDs between experiments at different distances from the cathode, as well as day-to-day, were below 10%.

Gas-kinetic temperature

The temporal behavior of the gas-kinetic temperature, at different distances from the cathode at 1 Torr and 3 Torr, is depicted in Figs. 3 and 4, respectively. The zero ms point on the time axis represents the onset of the glow-discharge pulse. Only scattering from the discharge axial position was observed and data closer than 4 mm from the cathode could not be obtained due to stray light from the cathode assembly. Fig. 3 (1 Torr) shows the gas-kinetic temperature rising as soon as 0.2 ms (450 K) after discharge initiation at distances close to the cathode (4 mm). Also at 4 mm, as well as 6 mm, it is interesting to see T_g increasing through the duration of the pulse until it reaches the maximum ($\sim$700 K at 4 mm). When we move farther away from the cathode ($\geq$8 mm) the maximum T_g is attained 2 ms into the pulse ($\sim$500 K at 8 mm). The T_g is also shown to decline as we move farther from the cathode and as soon as the pulse is terminated. The same trends can be observed at 3 Torr (Fig. 4), but with some exceptions. At 3 Torr the maximum T_g is on the order of 1000 K at 4 mm from the cathode. This is not unexpected since the current at 3 Torr is much higher than at 1 Torr and it has been shown that the gas-kinetic temperature is proportional to the glow-discharge power.[39,47] The main difference between the behavior at 1 and 3 Torr is in the time it takes for the maximum T_g to be realized. At 4 mm from the cathode in the 3 Torr discharge, T_g is already $\sim$850 K at 0.2 ms; by 0.6 ms the maximum T_g is reached. One might argue that this is due to the greater collision frequency at higher pressures. A more important contributor, however, is probably the temporal behavior of the current. It can be observed from Fig. 2E and 2F that the current trace at 3 Torr takes longer to return to its plateau value than at 1 Torr. It is likely this higher current causes an instantaneous raise in power which in turn results in higher gas-kinetic temperatures.

The plateau values of T_g at both pressures compare fairly well with those in previous continuous-dc glow discharge studies performed with the same laser scattering instrument, after considering the experimental differences in current and voltage.[38,39] In those investigations, the following values were obtained at 4 mm from the cathode: T_{gmax} = 825 K at 1 Torr, 10 mA, 880 V; T_{gmax} = 1025 K at 3 Torr, 65 mA, 1000 V. The difference in cathode temperature also deserves some consideration because it has been shown to exert a major influence on the resulting gas-kinetic temperature,[39] and lower cathode temperatures will exist under pulsed conditions. An extensive comparison of gas-temperature studies in dc analytical glow discharges can be found in our earlier manuscript.[38]

Pollman and co-workers[29] examined analytical μs- and ms-pulsed glow discharges and approximated the gas-kinetic temperature from rotational temperatures (T_{rot}) calculated from the R branch transitions of the N_2^+ first negative system band emission. The lowest T_{rot} was observed for a μs-pulsed glow discharge ($\sim$475 K) followed by ms-pulsed ($\sim$600 K) and the highest under dc conditions ($\sim$650 K). They also showed that after 1 ms, the ms-pulsed glow discharge starts resembling a dc discharge with respect to T_{rot} under their experimental conditions (1.5 Torr Ar, 0.3 Torr N_2; 0.25 W, ms-pulsed; 2.5 W, d.c.). Jackson and King[19] used the same approach to determine T_{rot} in a 5 ms pulsed glow discharge as a function of distance from the cathode. Under their experimental conditions (0.8 Torr Ar, 0.01 Torr N_2, 1.5 W peak) they observed the highest T_{rot} at the cathode ($\sim$850 K), with a steady decline farther from the cathode ($\sim$725 K at 5 mm). As mentioned above, the current and voltage have a strong influence on the measured temperatures and account for the discrepancies among the studies. One also has to take into account the size of the cathode, or cell geometry, because the current and power densities have an influence as well. In addition, the technique used for measuring temperature has an impact on the results. When the gas-kinetic temperature is approximated by the T_{rot} of a certain molecule (N_2^+, OH, *etc.*) there must be a sufficient number density of that molecule to obtain useful spectra. If these molecular species are not indigenous to the plasma they have to be introduced externally, which perturbs the plasma. It has been shown that adding increasing amounts of N_2 to a glow discharge causes the T_{rot} to drop accordingly.[48] Time resolution is also of concern. Jackson and King[19] did not report T_{rot} before 2 ms or after 5 ms due to insufficient signal strengths and because previous studies showed it takes 1–2 ms to reach spectroscopic equilibrium in ms-pulsed glow discharges.[17,29]

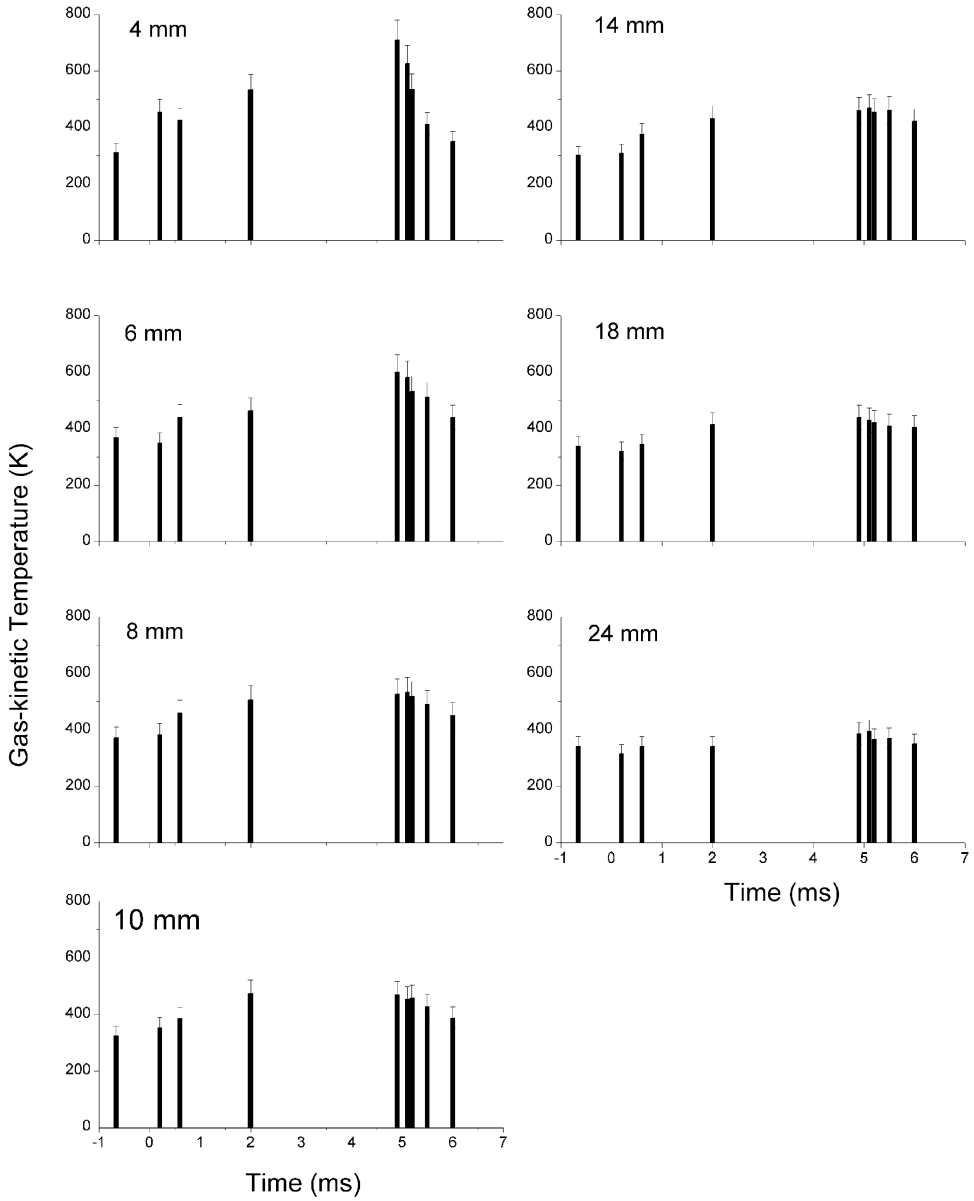

Fig. 3 Gas-kinetic temperatures as a function of time during the glow-discharge pulse at several distances from the cathode (1 Torr, 920 V plateau, 13 mA plateau).

In addition, they did not observe any significant differences between the time-resolved and time-averaged T_{rot} from 2 ms to 5 ms in the range of 0 mm to 5 mm from the cathode. In contrast, the present study shows the gas-kinetic temperature rising from 2 ms to 4.9 ms at 4 mm and 6 mm from the cathode (*cf.* Fig. 3). Yet another factor that may contribute to this disparity is cathode heating, which is affected by cooling efficiency and applied power[4] (higher power in our case).

The instrumentation used in the present study limits how close to the cathode one can measure T_g. In this respect, obtaining T_{rot} from the Boltzmann plot of N_2^+ emission has proven complementary to Rayleigh scattering. Overall, however, Rayleigh scattering has proven more powerful when time resolution in the μs/ms time regimes is needed. For example, with Rayleigh scattering the gas-kinetic temperature can be observed before the onset of the pulse (−0.6 ms), showing that in some cases T_g does not return completely to room temperature between pulses, especially at 3 Torr and closer to the cathode (*cf.* Figs. 3 and 4). This will have some impact on the spatial distribution of the gas breakdown in the subsequent pulse, which might affect prepeak characteristics. Also, with Rayleigh scattering the prepeak T_g can be observed and shown to be related to the temporal profiles of current. Furthermore, the observed afterpeak T_g gives an idea of how the mean free path changes with time as a function of distance from the cathode.

Electron properties

The electron behavior was followed by Thomson scattering with a multi-channel gated photon-counting technique. Only spectra at 1 Torr were obtained to facilitate comparison with

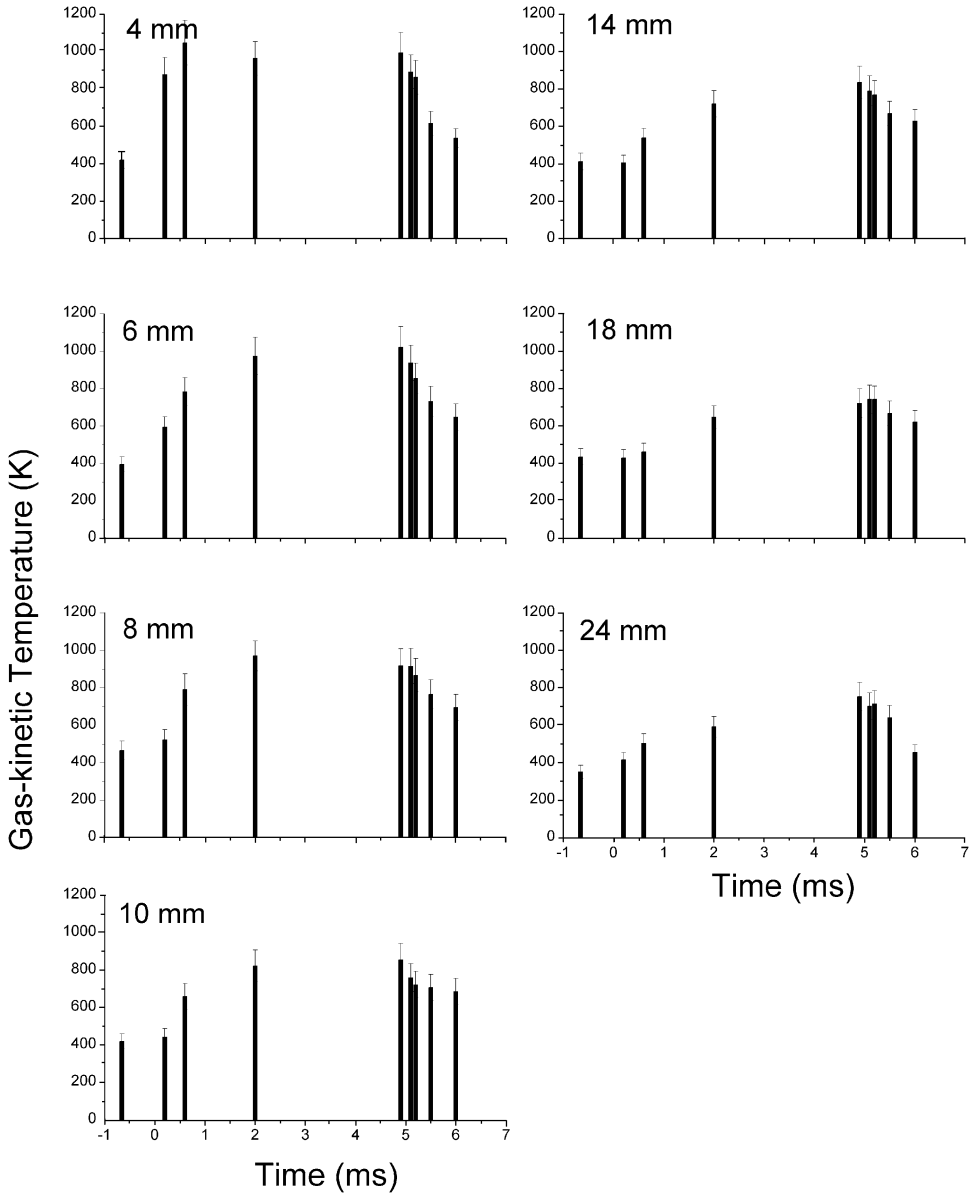

Fig. 4 Gas-kinetic temperatures as a function of time during the glow discharge pulse at several distances from the cathode (3 Torr, 920 V plateau, 75 mA plateau).

other fundamental and application studies of analytical ms-pulsed glow discharges, most of which are performed at ≤ 1 Torr. The low electron number densities found in analytical glow discharges results in weak Thomson-scattering signals. This situation requires not only the use of photon-counting techniques but also very long counting times. Also, the instrumentation used in this study allows only one wavelength channel to be observed at a time. Thus, in order to keep the measurements practical while holding drift to a minimum, a counting time of 20 min per wavelength channel (24 000 laser shots) was used. The resulting sputtering times were thus kept below six hours. This arrangement gave adequate signals to study the prepeak (0.2 ms), plateau (4.9 ms), and afterglow (5.1 ms and 5.2 ms) regions at 4 mm, 6 mm, and 8 mm from the cathode. The Rayleigh scattering calibration performed daily before and after the Thomson scattering experiment showed RSDs $< 5\%$ within the same day and $< 10\%$ from day-to-day.

In order to extract T_e from Thomson-scattering spectra the spectra were linearized by plotting the natural logarithm of the signal *versus* the square of the wavelength shift.[35] These linearized Thomson-scattering plots will result in a straight line if the electron energy distribution is Maxwellian; from the slope of that line, one can calculate T_e. However, previous studies have shown that the EEDF is non-Maxwellian in analytical glow discharges,[37,38,49] so linearized Thomson scattering spectra do not yield a single straight line, especially close to the cathode, but rather two distinct observable regions. A very good estimate of the energies of different electron groups can be obtained by assuming a bi-Maxwellian distribution, because each region gives a good linear fit ($R^2 \geq 0.9$). The

first few wavelength channels gave slopes corresponding to thermalized electron temperatures (0.26–0.31 eV) while the tails of the spectra gave slopes corresponding to higher-energy electrons (0.9–1.5 eV).[38] In the following section, the results referring to the thermalized electron group will be those coming from the first few wavelength channels of the Thomson-scattering spectra while the results referring to the higher-energy electron group will be those from the observable tails of the Thomson-scattering spectra.

Figs. 5–8 show the electron temperature and electron number density of both the thermalized electron group and the higher-energy group, as a function of radial position in the discharge at different distances from the cathode. The zero radial position corresponds to the discharge axis. Only half of the discharge was observed due to compromises made in magnification, solid angle, *f*-number matching, and space available. Nevertheless, radial resolution is maintained without any assumptions about symmetry.

Before discussing the electron temporal behavior let us examine the radial profiles. The thermalized electron temperatures (*cf*. Fig. 5) show little change. This is not the case for the higher-energy group, which shows a decrease in temperature from the discharge axis to the outer positions (*cf*. Fig. 7). On the other hand, both the thermalized and higher-energy groups show a drop in electron number density from the axis to the outer part of the discharge (*cf*. Figs. 6 and 8). Numerical simulations under continuous glow discharge conditions have shown that T_g is highest at the axial position even within the cathode area.[39] The decline in T_e and n_e as a function of radial position might be due to a higher number of collisions in the outer regions because of the higher Ar gas density (T_g is inversely proportional to the plasma gas density). In the case

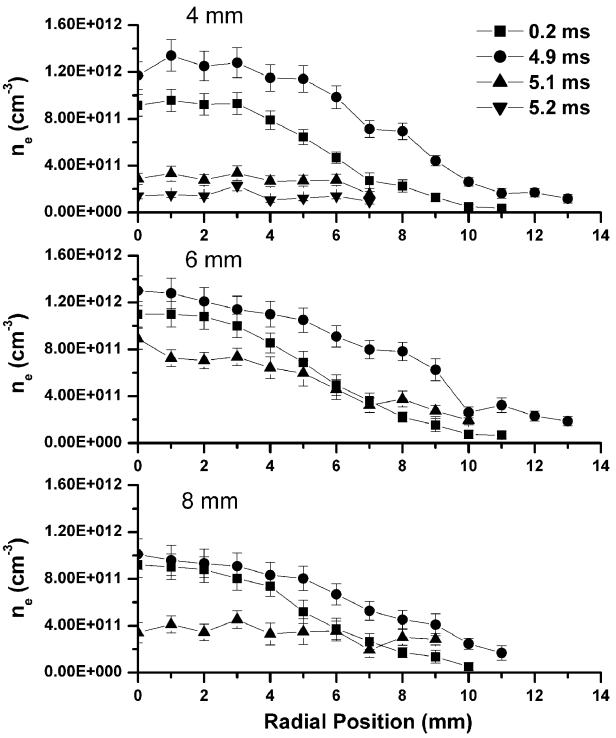

Fig. 6 Thermalized electron group number density as a function of discharge radial position at different distances from the cathode (1 Torr, 920 V plateau, 13 mA plateau). Error bars represent standard deviation.

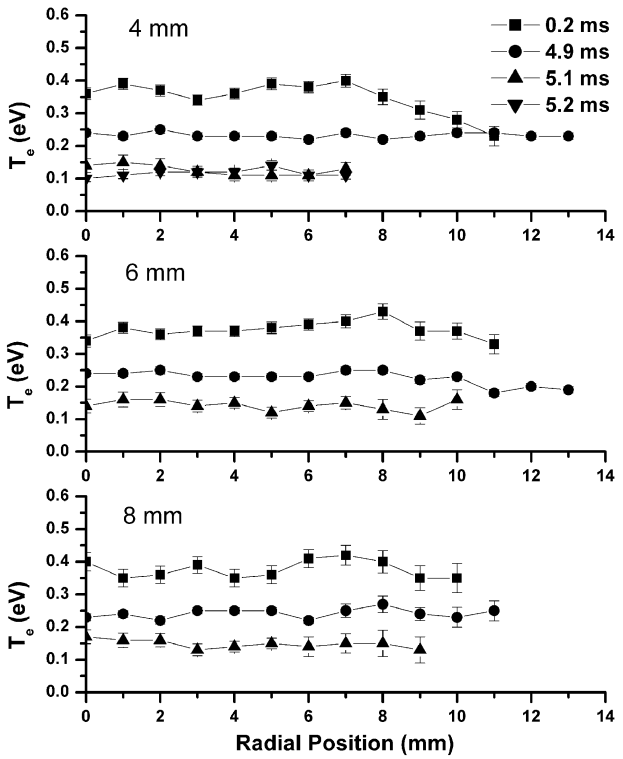

Fig. 5 Thermalized electron group temperature as a function of discharge radial position at different distances from the cathode (1 Torr, 920 V plateau, 13 mA plateau). Error bars represent standard deviation.

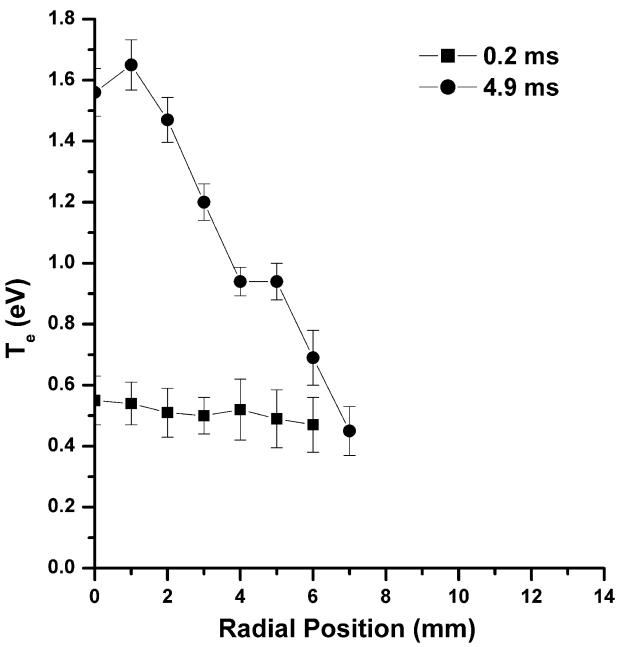

Fig. 7 'Higher-energy' electron group temperature as a function of discharge radial position at 4 mm from the cathode (1 Torr, 920 V plateau, 13 mA plateau). Error bars represent standard deviation.

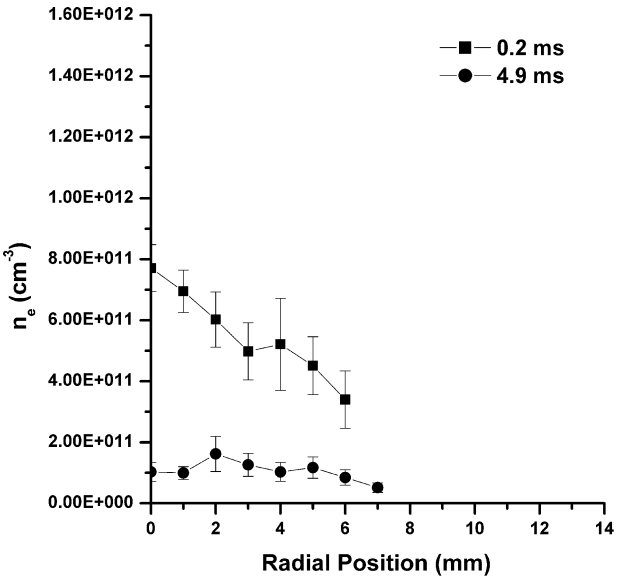

Fig. 8 'Higher-energy' electron group number density as a function of discharge radial position at 4 mm from the cathode (1 Torr, 920 V plateau, 13 mA plateau). Error bars represent standard deviation.

of the higher-energy electron group (*cf*. Fig. 7) the more pronounced radial profile structure at 4.9 ms, when compared to 0.2 ms, might be due to a larger Ar gas density gradient since T_g is higher at 4.9 ms.

Prepeak

Fig. 5 shows that the thermalized electron temperature in the prepeak (0.2 ms) is greater than during the plateau (4.9 ms). However, the electron number density is greater during the plateau than in the prepeak (Fig. 6). In contrast, the behavior is opposite for the high-energy electron group at 4 mm (Figs. 7 and 8), where a lower T_e and a higher n_e are observed during the prepeak when compared with the plateau. The thermalized electron number density and electron temperature do not seem to change significantly during the prepeak at different distances from the cathode. Sufficient signals to produce reliable electron fundamental parameters at 5.2 ms or for the higher-energy electron group could not be obtained under the current operating conditions at 6 mm or 8 mm from the cathode.

The temporal profile of the discharge voltage contributes greatly to the T_e behavior. At the beginning of the pulse the voltage takes some time to reach the plateau value (*cf*. Fig. 2). This slow rise in voltage will cause the primary electrons emitted from the cathode to be accelerated to lower velocities compared to in the plateau, where the applied voltage has reached its maximum value. This explains the lower T_e observed in the higher-energy electron group during the prepeak. In addition, the lower velocities of the primary electrons will result in more favorable energy-transfer cross-sections between the primary electrons and the secondary electrons, which arise from gas-phase ionization, *via* Coulombic interactions. This in turn explains the increase in T_e observed for the thermalized electron group during the prepeak compared to the plateau. A similar hypothesis was proposed by Klingler *et al*.[17] to explain the greater levels of plasma-gas ions and gas-impurity ions observed during the prepeak *via* ms-pulsed glow-discharge mass spectrometry. This is also consistent with the higher internal energies measured in thermometric species (tungsten carbonyl) during the prepeak as observed by Li and co-workers[25] in a ms pulsed radio frequency glow discharge.

Afterglow

As soon as the input pulse is terminated, the electron temperature is greatly reduced at 4 mm, 6 mm and 8 mm from the cathode (*cf*. Fig. 5). The electron number density also drops during the afterglow at the temporal positions studied here (5.1 ms and 5.2 ms, *cf*. Fig. 6). In general, during the pulse plateau the electron number density goes down as we move farther from the cathode. However, as opposed to the plateau, the n_e at 5.1 ms increases from 4 mm to 6 mm from the cathode and the afterglow (5.2 ms) to plateau (4.9 ms) n_e ratio is greater at 8 mm than at 4 mm.

There are several processes that need to be taken into account in order to explain the observations above. First, as shown in Fig. 5, as soon as the input pulse is terminated, electrons rapidly lose energy because there is no longer a driving potential to accelerate them; subsequent collisions result in their eventual thermalization with the gas.[50] Thus, a substantial reduction in diffusion-based electron loss will accompany the drop in energy.[50] In addition, the argon metastable population has been shown to increase at certain spatial/temporal positions in the afterglow.[16,20] Therefore, the rise in the afterglow/plateau n_e at positions farther from the cathode might be caused, in part, by a larger population of argon metastables that undergo Penning ionizations at such spatial positions. In fact, greater argon metastable populations have been observed at certain instances in the afterglow at 6 mm than at 4 mm from the cathode.[20] This trend is also consistent with numerical modeling of a ms-pulsed glow discharge, where the argon metastable population was seen to be lower at 4 mm compared with 6 mm from the cathode from 5.1 ms to 5.4 ms into the afterglow.[22]

The formation of argon metastables during the afterglow has been proposed to be due to electron-ion recombination followed by radiative decay.[20,22] Bogaerts and co-workers[22] calculated n_e with a numerical modeling network that predicted n_e declining upon pulse termination; however, they point out that their results might not be realistic because they cannot explain the high rate of recombination. Based on the present study, however, their results seem more realistic. Bogaerts, *et al*. estimated the electron density required to account for electron-ion recombination rates in collisional–radiative models and indicated that n_e would have to go up considerably in the afterglow in comparison with the plateau for this mechanism to hold. They pointed to collisional–radiative recombination as the most plausible mechanism based on assumptions of Ar^+ and Ar_2^+ ion densities, and an electron temperature thermalizing to $\sim$0.05 eV within the first 100 μs of the afterglow.

Biondi[50,51] studied the electron number densities in afterglows of pulsed magnetron discharges by means of microwave techniques. His results showed that the electron number

density climbs in the afterglow of a He (3.1 mm Hg) magnetron discharge by as much as a factor of two and for a Ne (1.56 mm Hg) magnetron by as much as a factor of ~1.5. An increase in n_e is also observed for a He magnetron discharge containing 0.115% Ar, but the electron number density for a pure Ar magnetron afterglow was not reported. Greenberg and Hebner[52] also measured n_e in pulsed rf discharges (gaseous electronics conference reference cell, GEC) *via* microwave interferometry in pure He and pure Ar. An increase of almost a factor of 3 was observed for the electron number density in the afterglow in the He case (75 V, 1 Torr), which is consistent with Biondi.[50] On the other hand, they did not observe the same behavior for Ar under any of the power and pressure conditions studied. Further, Overzet and Kleber[53] compared microwave-interferometry and Langmuir-probe techniques to measure the electron properties in pulsed GEC discharges under pure He or pure Ar. In accordance with the above-mentioned studies, they observed a n_e elevation of more than a factor of three in the afterglow of the pure He discharge, whereas the n_e values were consistently lower in the afterglow of the pure Ar discharge than during the plateau. They also addressed the significance of the contribution of reactions between metastables to yield energetic electrons. High-energy electrons were confirmed by studies of the EEDF during the afterglow, where peaks at ~15 eV and ~7.5 eV were observed for He and Ar, respectively. These reactions are as follows:

$$Ar^* + Ar^* \rightarrow Ar^+ + Ar + e^- \text{ (7.3 eV–7.9 eV)}$$
$$He^* + He^* \rightarrow He^+ + He + e^- \text{ (15.05 eV–16.65 eV)}$$

In the present study, the EEDF at these high energies could not be followed because the corresponding electron number densities are below the detection limits of the instrument under the experimental conditions that were employed. Nevertheless, Strauss *et al.* [16] had already pointed toward the significance of these reactions in pulsed hollow cathode discharges.

The results of the present study (*cf.* Figs. 5 and 6) are consistent with those of Greenberg and Hebner,[52] as well as those of Overzet and Kleber.[53] The elevation in electron number density during the afterglow of a He pulsed discharge, as opposed to their loss in an Ar pulsed discharge, might be caused by several factors. It has been observed that the electron temperature drops much more rapidly in the afterglow of a He discharge than in an Ar discharge.[53] This might be partly due to the smaller mass of the He atom, which facilitates electron cooling *via* elastic collisions. In addition, in the afterglow, the high thermal conductivity of He will probably cause the gas-kinetic temperature to go down much faster than in Ar (*cf.* Fig. 2). This difference, in turn, might play a role because the electrons eventually thermalize to the gas-kinetic temperature. Thus, the differences in T_g observed in the afterglow as a function of distance from the cathode might also influence the spatial behavior of T_e and n_e. In this fashion, ambipolar diffusion could be higher for a longer period of time in Ar (and at distances closer to the cathode) because the electron temperature remains elevated and will lead to a greater loss rate of electrons.[53]

The results of the present study, however, bring into question the significance of the collisional–radiative recombination mechanism for the formation of Ar metastables. An alternative mechanism, as proposed by Bogaerts *et al.*,[22] is dissociative recombination with molecular ions in highly vibrational levels

$$e^- + Ar_2^+ \rightarrow Ar^* + Ar$$

After their studies of microwave-discharge afterglows, Biondi and co-workers[54–57] also proposed dissociative recombination as one of the most likely mechanisms under conditions where Ar_2^+ formation was sufficiently high (*e.g.*, at Ar pressures of ~10 mm Hg), for example *via* a three body reaction

$$Ar^+ + Ar + Ar \rightarrow Ar_2^+ + Ar$$

Regardless, more experimental data under analytical pulsed glow discharge conditions is clearly needed for further consideration of this path. An additional alternative worth noting is the possible contribution of Ar Rydberg states, since these highly excited neutrals have been proposed to play a significant role in the formation of Ar* in a fast-flowing glow discharge, especially in the presence of contaminant gases.[58–61] Unfortunately, the current understanding of Rydberg species in analytical pulsed glow discharges is very limited. Certainly, all of these mechanisms demand further investigation.

Future work in our laboratories includes additional studies into the above-mentioned mechanisms, as well as investigating the effects of impurity trace gases on the fundamental parameters of pulsed dc glow discharges.

Acknowledgements

The authors gratefully acknowledge support by the US Department of Energy through Grant DE-FG02-98ER14890. Gerardo Gamez would like to acknowledge financial support from an American Chemical Society Division of Analytical Chemistry fellowship and a fellowship from MERCK Research Laboratories.

References

1 R. Payling, D. G. Jones and A. Bengtson, *Glow Discharge Optical Emission Spectrometry*, John Wiley & Sons Ltd., Chichester, 1997.
2 T. Nelis and R. Payling, *Glow Discharge Optical Emission Spectroscopy: A Practical Guide*, Royal Society of Chemistry, Cambridge, 2003.
3 R. K. Marcus and J. A. C. Broekaert, *Glow Discharge Plasmas in Analytical Spectroscopy*, John Wiley & Sons Ltd., Chichester, 2003.
4 A. Bogaerts and R. Gijbels, *J. Anal. At. Spectrom.*, 2004, **19**, 1206–1212.
5 M. Kasik, C. Michellon and L. C. Pitchford, *J. Anal. At. Spectrom.*, 2002, **17**, 1398–1399.
6 G. J. M. Hagelaar and L. C. Pitchford, *J. Anal. At. Spectrom.*, 2002, **17**, 1408–1410.
7 W. W. Harrison, *J. Anal. At. Spectrom.*, 1998, **13**, 1051–1056.
8 W. W. Harrison, W. Hang, X. Yan, K. Ingeneri and C. Schilling, *J. Anal. At. Spectrom.*, 1997, **12**, 891–896.
9 W. W. Harrison, C. Yang and E. Oxley, *Anal. Chem.*, 2001, **73**, 480A–487A.
10 C. L. Lewis, E. S. Oxley, C. K. Pan, R. E. Steiner and F. L. King, *Anal. Chem.*, 1999, **71**, 230–234.
11 C. L. Lewis, M. A. Moser, D. E. Dale Jr., W. Hang, C. Hassell, F. L. King and V. Majidi, *Anal. Chem.*, 2003, **75**, 1983–1996.
12 V. Majidi, M. Moser, C. Lewis, W. Hang and F. L. King, *J. Anal. At. Spectrom.*, 2000, **15**, 19–25.

13 C. L. Lewis, M. A. Moser, W. Hang, D. E. Dale Jr., D. C. Hassell and V. Majidi, *J. Anal. At. Spectrom.*, 2003, **18**, 629–636.
14 R. E. Steiner, C. L. Lewis and V. Majidi, *J. Anal. At. Spectrom.*, 1999, **14**, 1537–1541.
15 D. Fliegel, R. Waddell, V. Majidi, D. Guenther and C. L. Lewis, *Anal. Chem.*, 2005, **77**, 1847–1852.
16 J. A. Strauss, N. P. Ferreira and H. G. C. Human, *Spectrochim. Acta, Part B*, 1982, **37**, 947–954.
17 J. A. Klingler, C. M. Barshick and W. W. Harrison, *Anal. Chem.*, 1991, **63**, 2571–2576.
18 C. L. Lewis, L. Li, J. T. Millay, S. Downey, J. Warrick and F. L. King, *J. Anal. At. Spectrom.*, 2003, **18**, 527–532.
19 G. P. Jackson and F. L. King, *Spectrochim. Acta, Part B*, 2003, **58**, 185–209.
20 G. P. Jackson, C. L. Lewis, S. K. Doorn, V. Majidi and F. L. King, *Spectrochim. Acta, Part B*, 2001, **56**, 2449–2464.
21 C. Pan and F. L. King, *J. Am. Soc. Mass Spectrom.*, 1993, **4**, 727–732.
22 A. Bogaerts, R. Gijbels and G. P. Jackson, *J. Anal. At. Spectrom.*, 2003, **18**, 533–548.
23 A. Bogaerts and R. Gijbels, *J. Anal. At. Spectrom.*, 2001, **16**, 239–249.
24 C. L. Lewis, G. P. Jackson, S. K. Doorn, V. Majidi and F. L. King, *Spectrochim. Acta, Part B*, 2001, **56**, 487–501.
25 L. Li, J. T. Millay, J. P. Turner and F. L. King, *J. Am. Soc. Mass Spectrom.*, 2004, **15**, 87–102.
26 F. Richter, T. Welzel, T. Dunger and H. Kupfer, *Surf. Coat. Technol.*, 2004, **188–189**, 384–391.
27 R. Hugon, G. Henrion and M. Fabry, *Surf. Coat. Technol.*, 1993, **59**, 82–85.
28 R. Hugon, G. Henrion and M. Fabry, *Plasma Sources Sci. Technol.*, 1996, **5**, 553–559.
29 D. Pollmann, K. Ingeneri and W. W. Harrison, *J. Anal. At. Spectrom.*, 1996, **11**, 849–853.
30 I. H. Hutchinson, *Principles of Plasma Diagnostics*, Cambridge University Press, Cambridge, 2002.
31 A. Bogaerts, A. Quentmeier, N. Jakubowski and R. Gijbels, *Spectrochim. Acta, Part B*, 1995, **50**, 1337–1349.
32 M. Huang and G. M. Hieftje, *Spectrochim. Acta, Part B*, 1985, **40**, 1387–1400.
33 G. M. Hieftje, *Spectrochim. Acta, Part B*, 1992, **47**, 3–25.
34 M. Katsunori, U. Kiichiro, B. Mark and M. Mitsuo, *Purazuma, Kaku Yugo Gakkaishi*, 2000, **76**, 7–18.
35 K. Warner and G. M. Hieftje, *Spectrochim. Acta, Part B*, 2002, **57**, 201–241.
36 K. Muraoka, K. Uchino, Y. Yamagata, Y. Noguchi, M. Mansour, P. Suanpoot, S. Narishige and M. Noguchi, *Plasma Sources Sci. Technol.*, 2002, **11**, A143–A149.
37 G. Gamez, M. Huang, S. A. Lehn and G. M. Hieftje, *J. Anal. At. Spectrom.*, 2003, **18**, 680–684.
38 G. Gamez, A. Bogaerts, F. Andrade and G. M. Hieftje, *Spectrochim. Acta, Part B*, 2004, **59**, 435–447.
39 A. Bogaerts, R. Gijbels, G. Gamez and G. M. Hieftje, *Spectrochim. Acta, Part B*, 2004, **59**, 449–460.
40 J. van der Mullen, G. Boidin and M. van de Sandea, *Spectrochim. Acta, Part B*, 2004, **59**, 929–940.
41 A. Kono and K. Nakatani, *Rev. Sci. Instrum.*, 2000, **71**, 2716–2721.
42 S. A. Moshkalyov, C. Thompson, T. Morrow and W. G. Graham, *J. Vac. Sci. Technol., A*, 2000, **18**, 1395–1400.
43 N. N. Sesi, D. S. Hanselman, P. Galley, J. Horner, M. Huang and G. M. Hieftje, *Spectrochim. Acta, Part B*, 1997, **52**, 83–102.
44 K. Suhling, G. Hungerford, R. W. Airey and B. L. Morgan, *Meas. Sci. Technol.*, 2001, **12**, 131–141.
45 X. Tian, B. Tang and P. K. Chu, *J. Appl. Phys.*, 1999, **86**, 3567–3570.
46 M. J. Goeckner and C. E. Van Wagoner, Varian Semiconductor Equipment Associates, Inc., USA, Application: WO, 2001.
47 A. Bogaerts, R. Gijbels and V. V. Serikov, *J. Appl. Phys.*, 2000, **87**, 8334–8344.
48 S. K. Ohorodnik and W. W. Harrison, *J. Anal. At. Spectrom.*, 1994, **9**, 991–996.
49 D. Fang and R. K. Marcus, *Spectrochim. Acta, Part B*, 1990, **45**, 1053–1074.
50 M. A. Biondi, *Phys. Rev.*, 1952, **88**, 660–665.
51 M. A. Biondi, *Rev. Sci. Instrum.*, 1951, **22**, 500–502.
52 K. E. Greenberg and G. A. Hebner, *J. Appl. Phys.*, 1993, **73**, 8126–8133.
53 L. J. Overzet and J. Kleber, *Plasma Sources Sci. Technol.*, 1998, **7**, 512–523.
54 M. A. Biondi and T. Holstein, *Phys. Rev.*, 1951, **82**, 962–963.
55 M. A. Biondi, *Phys. Rev.*, 1951, **83**, 1078–1080.
56 M. A. Biondi, *Phys. Rev.*, 1963, **129**, 1181–1188.
57 W. A. Rogers and M. A. Biondi, *Phys. Rev.*, 1964, **134**, 1215–1225.
58 R. S. Mason, P. D. Miller and I. P. Mortimer, *Phys. Rev. E: Stat. Phys., Plasmas, Fluids, Relat. Interdiscip. Top.*, 1997, **55**, 7462–7472.
59 R. S. Mason, P. D. Miller, I. Mortimer, D. J. Mitchell and N. A. Dash, *Phys. Rev. E: Stat., Nonlinear, Soft Matter Phys.*, 2003, **68**, 016408/016401–016408/016414.
60 K. Newman, R. S. Mason, D. R. Williams and I. P. Mortimer, *J. Anal. At. Spectrom.*, 2004, **19**, 1192–1198.
61 R. S. Mason, D. R. Williams, I. P. Mortimer, D. J. Mitchell and K. Newman, *J. Anal. At. Spectrom.*, 2004, **19**, 1177–1185.